PROCEEDINGS OF SCIENCE

Recent Results from the Cosmic Ray Isotope Spectrometer on NASA's Advanced Composition Explorer

M. E. Wiedenbeck[*a], **W. R. Binns**[b], **M. H. Israel**[b], **R. A. Leske**[c], **E. R. Christian**[d], **C. M. S. Cohen**[c], **A. C. Cummings**[c], **A. J. Davis**[c], **G. A. de Nolfo**[d], **A. W. Labrador**[c], **K. A. Lave**[b], **R. A. Mewaldt**[c], **E. C. Stone**[c], **and T. T. von Rosenvinge**[d]

[a] *Jet Propulsion Laboratory, California Institute of Technology, Pasadena, CA 91109 USA*
[b] *Washington University, St Louis, MO 63130 USA*
[c] *California Institute of Technology, Pasadena, CA 91125 USA*
[d] *NASA / Goddard Space Flight Center, Greenbelt, MD 20771 USA*
E-mail: `mark.e.wiedenbeck@jpl.nasa.gov`

The Advanced Composition Explorer (ACE), which carries instrumentation for making high-precision measurements of the charge and mass of energetic nuclei between ∼1 keV/nuc and ∼1 GeV/nuc, was launched in August 1997 into an orbit about the L1 Lagrangian point 1.5 million km sunward of the Earth. From this vantage point, ACE collects data that are used for a wide range of studies in galactic and heliospheric physics. The ACE spacecraft and instruments are, for the most part, continuing to perform very well and to extend their data sets. The long mission duration, which is already almost an order of magnitude greater than the two years that was nominally required of ACE, has made it possible to address science topics beyond those envisioned when the mission was proposed. In this paper we address several topics to which ACE's Cosmic Ray Isotope Spectrometer (CRIS) is contributing in the area of galactic cosmic radiation. CRIS has been able to make measurements of extremely rare species, including the primary radioactive nuclide ^{60}Fe and a number of stable "ultraheavy" elements with atomic numbers in the range $Z = 30$ to 40. In addition, elemental energy spectra have now been measured over a significant fraction of two solar cycles, thereby enabling studies of the time dependence of the solar modulation of galactic cosmic rays.

35th International Cosmic Ray Conference — ICRC2017
10–20 July, 2017
Bexco, Busan, Korea

---

[*] Speaker.

PoS(ICRC2017)1089

1. Introduction

The Advanced Composition Explorer (ACE) mission was developed in the 1990s under NASA's Explorer Program to carry out detailed investigations of the elemental, isotopic, and charge-state composition of energetic particle populations accelerated at the Sun, in the heliosphere, and in our Galaxy. The mission, its science objectives, and its payload of instruments are described in a series of articles published shortly after the 1997 launch [1]. Figure 1 shows a photograph of the spacecraft during integration at the Johns Hopkins Applied Physics Laboratory (APL) in 1996.

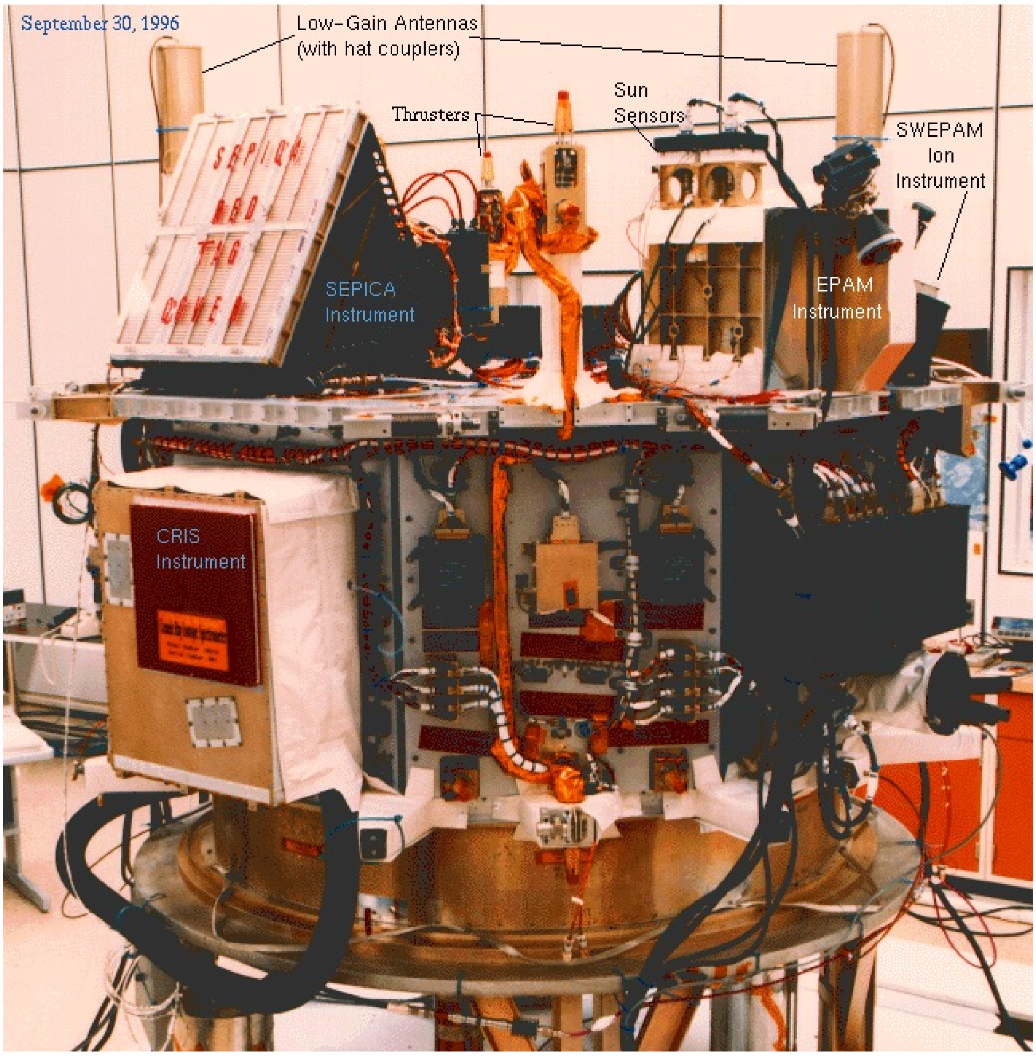

Figure 1: Photograph of the ACE spacecraft at APL after instrument integration and before installation of thermal blankets. On orbit, the top deck, where instruments used for studying the solar wind and solar energetic particles are mounted, faces generally sunward. The CRIS instrument is located on a side panel. Figure from the ACE Science Center Picture Gallery.

The highest energy measurements are made by the Cosmic Ray Isotope Spectrometer (CRIS) [2], which is used for the study of galactic cosmic rays (GCRs) that arrive near Earth with energies generally in the range ∼50 to ∼500 MeV/nuc. A schematic cross section of the instrument is shown in the left-hand panel of Figure 2. CRIS consists of four stacks of silicon solid-state detectors (two stacks are visible in Figure 2) that are used for making measurements of energy loss (ΔE) and residual energy (E') of nuclei that stop in those stacks. The right-hand panel in Figure 2 shows a sample of CRIS data illustrating how particle species are resolved on a plot of ΔE versus E'. This ΔE versus E' technique (also called dE/dx versus total-E) has been employed in numerous instruments designed for studying energetic particles in space.

The energy coverage for stopping particles is determined by the joint requirements that they penetrate to the second detector (E2) in one of the stacks and that they stop somewhere between E2 and E8 in that stack and do not trigger a back anticoincidence detector (E9) or any of the guard rings that surround detectors E2 through E7. At the front of the silicon detector stacks, CRIS has a scintillating optical fiber hodoscope (SOFT) sensor that provides measurements of the trajectories of particles incident on those stacks and allows precise corrections for the the amount of silicon penetrated in the stack detectors. Some examples of CRIS data on GCR elemental and isotopic composition can be found in [3, 4].

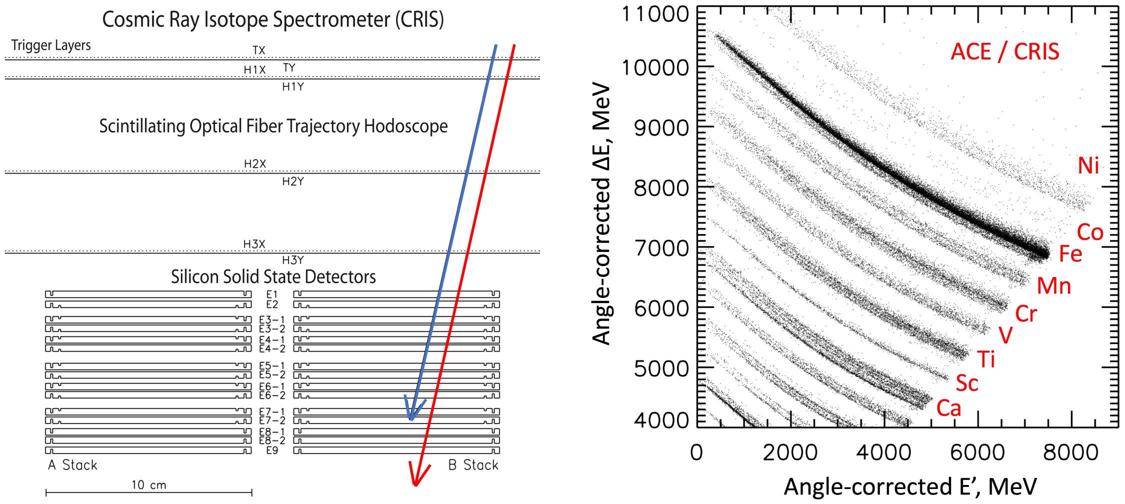

Figure 2: Left: cross section of the CRIS sensor system. Blue (red) arrow indicates the trajectory of a typical stopping (penetrating) particle. Figure adapted from [3]. Right: sample CRIS ΔE versus E' plot (including approximate corrections for incidence angle) showing separation of element and isotope tracks.

Although ACE was developed for a prime mission of 2-year duration, the design carefully avoided compromises that might unnecessarily limit the mission life time. At the time of this writing, ACE has been operating for just over 20 years and most of the instruments continue to perform well. In particular, the CRIS response has remained essentially unchanged since launch.

The long exposure time has enabled a variety of ACE studies that go beyond what was planned for the prime mission. With nearly two full solar cycles of data (one Hale magnetic cycle), it has been possible to trace how the solar modulation of both galactic cosmic rays and anomalous cosmic rays (ACRs) responds to solar variations. Figure 3 gives an overview of the variations seen in solar energetic particles (SEPs), ACRs, and GCRs over the course of the mission.

The long period of data collection has also allowed the accumulation of statistically meaningful samples of some rare elements and isotopes that led to new results on cosmic-ray composition.

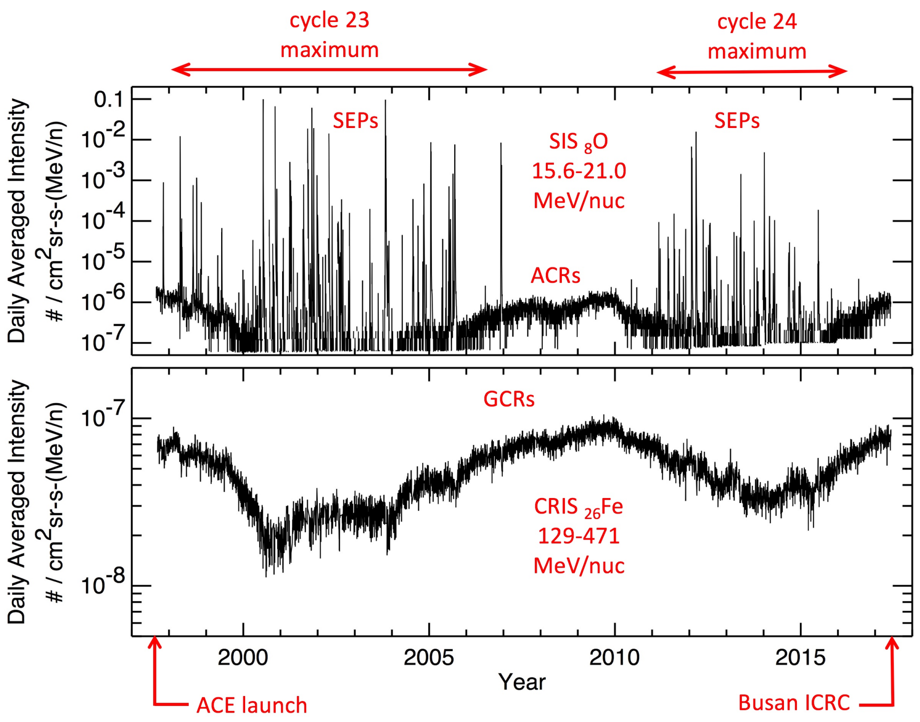

Figure 3: Energetic particle intensity variations measured over 20 years by instruments on ACE. Upper panel: 15.6–21.0 MeV/nuc oxygen measured by the Solar Isotope Spectrometer (SIS) [5] is dominated by large SEP events (intensity spikes) during the maxima of solar cycles 23 and 24 and by anomalous cosmic rays during solar minima. Lower panel: 426–466 MeV/nuc iron measured by the Cosmic Ray Isotope Spectrometer (CRIS) is dominated by galactic cosmic rays that have undergone solar modulation as they penetrated to the inner heliosphere.

Figure 4 shows how the fluence of GCR Fe collected by CRIS in three different energy intervals has grown over time. Now, in 2017, we are in the early part of another solar minimum period when the accumulated fluence increases most rapidly. By the time of the solar cycle 25 maximum, the GCR sample should exceed that obtained during the prime mission by more than an order of magnitude.

2. Primary Radioactive Nuclides: ^{60}Fe and ^{59}Ni

Binns et al. [6] have reported the first observations of a surviving primary radionuclide in the galactic cosmic rays. The isotope ^{60}Fe undergoes decay by β^- emission with a half-life of 2.6 Myr. Unlike radionuclides such as ^{10}Be or ^{26}Al, which have been extensively studied in cosmic rays, ^{60}Fe is not produced in significant abundance by fragmentation of heavier nuclides. Thus, any observed ^{60}Fe provides strong evidence that there is at least a component of the cosmic rays arriving near Earth that has been synthesized and ejected from stars on a time scale not significantly longer than several Myr.

Figure 5 shows a mass histogram containing Fe events measured during the first 17 years of the ACE mission. Besides the isotopes with masses 54 through 58, which were previously studied, this new, high-statistics sample reveals a peak centered around mass 60 that contains 15 events. Because

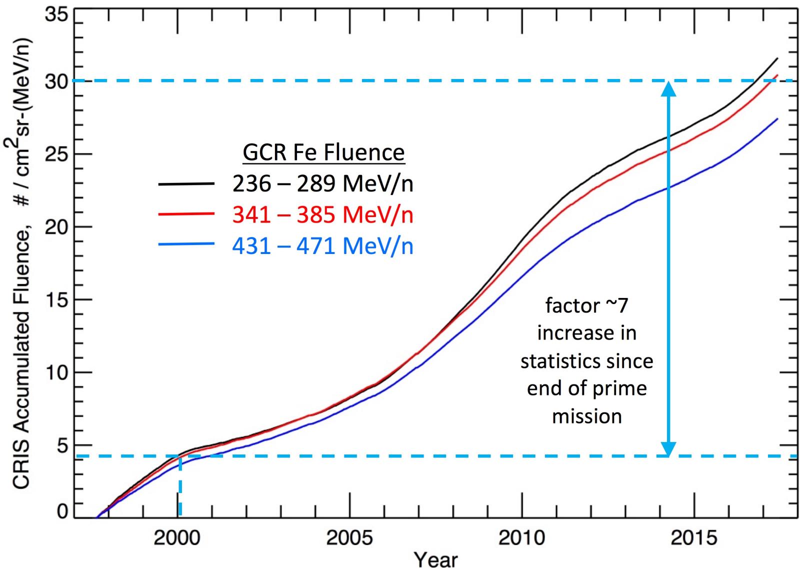

Figure 4: Galactic cosmic ray fluence measured in three energy intervals by CRIS from the start of the ACE mission through mid-2017. Since the completion of the prime mission in 2000, the size of the accumulated cosmic-ray sample has increased by a factor ∼7, enabling studies of some very low-abundance elements and isotopes.

of the long-term stability of the CRIS detectors and electronics and multiparameter measurements that allow efficient rejection of backgrounds (for example, due to fragmentation in the detector stacks) the collection of less than one ^{60}Fe event per year is sufficient to give a well-defined mass peak and enable measurement of the surviving ^{60}Fe abundance. The clean separation from the ^{58}Fe peak is possible because the isotope ^{59}Fe, which decays by β^- emission with a half-life of 45 days, is absent and because measured mass peaks typically do not have long tails on the high-mass side. Binns et al. [6] pointed out that the CRIS Co mass histogram (right-hand panel of Figure 5) for this same time period has only one event located two mass units above the heaviest stable nuclide, ^{59}Co, which has an abundance comparable to that of ^{58}Fe. They also carried out numerous tests that demonstrate that the ^{60}Fe events are a sample of the same arriving cosmic-ray population as the rest of the Fe.

In order to have confidence that the events identified as ^{60}Fe are not a background due to some much more abundant nuclide, we have looked in detail at the tails of the measured mass distributions. It is typical for the mass distributions measured with CRIS to have significantly more prominent tails on the low side than on the high side of the peaks, as can be seen in the right-hand panel of Figure 5 by comparing the low-side tail on ^{57}Co with the high-side tail on ^{59}Co. A major contributor to low-side tails is channeling, which causes particles traveling in directions closely aligned with major axes or planes of the silicon crystal to have a slightly reduced rate of energy loss. This effect causes a small decrease in the energy deposited in the ΔE detector and a corresponding increase in the following E' detector, which results in displacing an event toward the low-mass side of an isotope track. The left-hand panel of Figure 6 shows measured X and Y coordinate displacements (proportional to tangents of the corresponding projections of particle

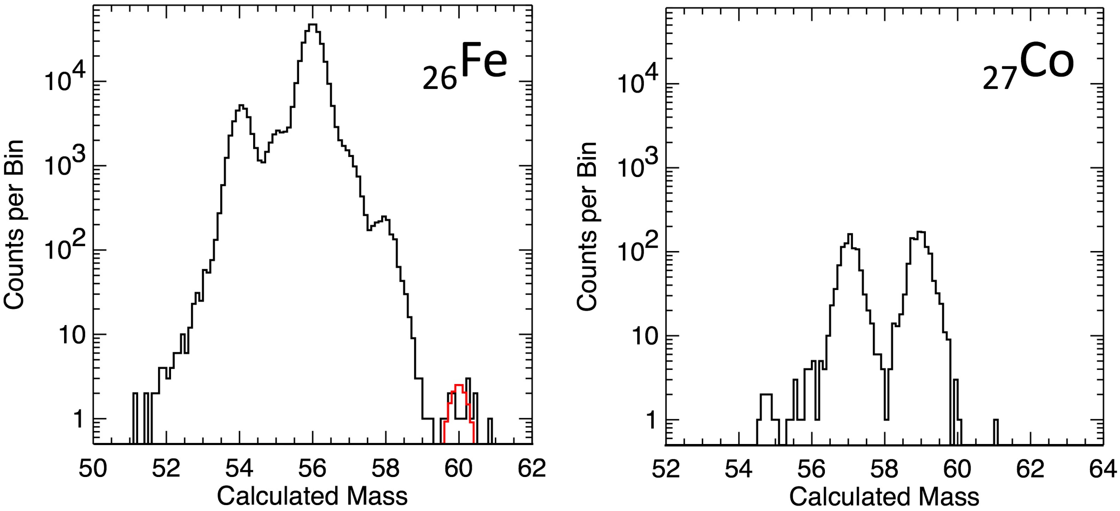

Figure 5: Left panel: histogram of calculated masses of cosmic-ray Fe nuclei measured with the ACE/CRIS instrument [6]. The red curve overlaid on the black histogram is a copy of the ^{56}Fe peak that has been shifted upward by 4 mass units and scaled down to have an area corresponding to the number of events in the ^{60}Fe region of the plot. Right panel: histogram of calculated masses of cosmic-ray Co nuclei.

incidence angles) measured for Fe nuclei traversing the SOFT hodoscope and falling in the low-side tail on the distribution of calculated charges ($Z < 25.65$). The pattern clearly demonstrates the importance of channeling in causing this tail.

In the ΔE versus E' technique employed in CRIS, response tracks of low-mass isotopes for an element of atomic number Z can lie close to the high-mass tracks for the adjacent element with atomic number $Z-1$. For ^{60}Fe, it is important that the boundary between Fe and Co be appropriately placed so that the low-side Co tail will not contribute background on the high side of the Fe distribution. The right-hand panel of Figure 6, which shows the calculated locations of tracks for selected Fe and Co isotopes in one of the CRIS detector combinations, indicates that a Co mass of ∼53.5 should overlap with ^{60}Fe. Fortunately, the ^{57}Co tail does not extend below mass ∼54.5 (Fig 5). It is conceivable, however, that the one event in the Fe mass histogram above mass 60.8 might actually be spillover from Co. This possibility was taken into account in the uncertainty assigned to the number of detected ^{60}Fe [6].

In addition to setting a limit on how long ago the arriving ^{60}Fe was synthesized, the detection of this radioisotope also provides a constraint on the distance to the sources where the nucleosynthesis occurred. Estimates of the diffusion coefficient that controls the transport of cosmic rays in the Galaxy have been derived from measurements of abundances of secondary radionuclides [7, 8]. Combining the diffusion coefficient with the time scale from the ^{60}Fe measurements, one can infer that the nucleosynthesis occurred no more than ∼1 kpc from the solar system.

The derivation of the source ratio ^{60}Fe/^{56}Fe depends significantly on the interstellar propagation model, with longer propagation times requiring larger source abundances of ^{60}Fe to leave the observed amount of this radionuclide after decay. Our simple leaky-box calculation [6] would be applicable if the ^{60}Fe were produced near the solar system and transported to us without spending

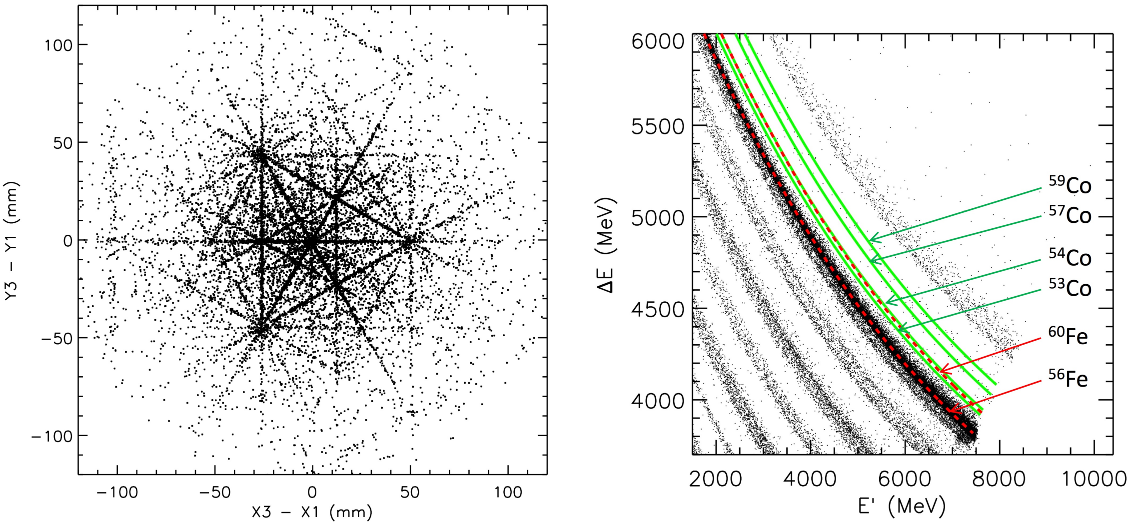

Figure 6: Left: two-dimensional distribution of incidence directions for Fe nuclei in the extreme low-side tail of the distribution of calculated charges ($Z < 25.65$ charge units). These events fall preferentially along low-order crystal planes of the $\langle 111 \rangle$ Si detectors. Right: calculated ΔE–E' tracks for selected stable and long-lived nuclides (^{56}Fe, ^{60}Fe, ^{57}Co, ^{59}Co) and for unstable nuclides that would overlap with the ^{60}Fe track if they were present (^{53}Co, ^{54}Co) superimposed on a sample of CRIS data. Typically, multiple mass measurements from this type of analysis are compared for consistency and averaged to optimize mass resolution and background rejection.

significant amounts of time in the galactic halo or in other distant regions. On the other hand, if ^{60}Fe is produced with the same spatial distribution as stable nuclides such as ^{56}Fe and spends a significant amount of time diffusing in the halo like secondary radionuclides, then a much larger fraction of the accelerated ^{60}Fe would have decayed.

Binns et al. [6] pointed out the possible association of the cosmic-ray ^{60}Fe being measured in CRIS with recently reported ^{60}Fe detected in deep-sea sediments and in samples of the lunar regolith (reviewed in [9]), which are thought to be due to deposition of ejecta from a recent, nearby supernova—perhaps the same supernova that produced the ^{60}Fe that CRIS is detecting.

Figure 7, taken from one of the earliest CRIS publications, shows no evidence for surviving ^{59}Ni in the arriving cosmic rays [10]. This nuclide is radioactive and its only significant decay mode is orbital electron capture (ec). As noted by Soutoul et al. [11], pure ec nuclides that are ejected in supernova explosions can provide an indication of the time delay between nucleosynthesis and acceleration. Until they are accelerated, these nuclei will have electrons attached and be able to decay, but after acceleration the ec decay is not possible and they become stable. The absence of ^{59}Ni (laboratory half-life of 7.6×10^4 yr) in the arriving cosmic rays indicates a long time delay, $\gtrsim 10^5$ yr, incompatible with the acceleration of the ^{59}Ni-containing ejecta by a shock wave from the same supernova that synthesized this material. The observed ^{59}Co was interpreted [10] as having dominantly been produced by the decay of ^{59}Ni, with a small admixture of secondaries produced by the spallation of heavier nuclides (primarily ^{60}Ni).

However, we noted that ^{59}Ni would also be absent if this nuclide were not produced and ejected in significant abundance from the supernova. Plots illustrating our interpretation of the CRIS ^{59}Ni

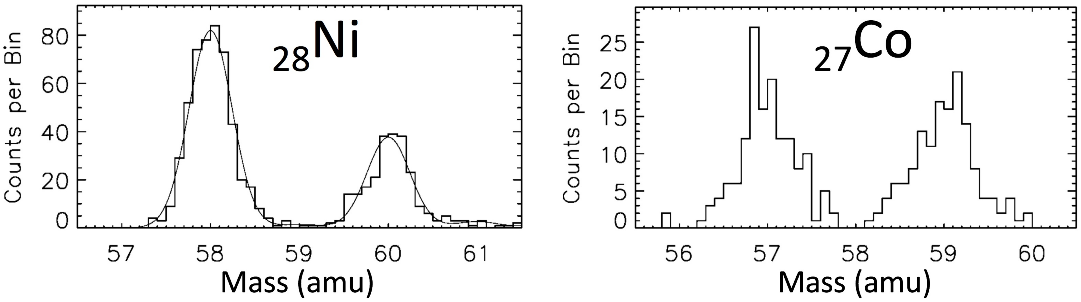

Figure 7: CRIS mass histograms for Ni (left) and Co (right). The isotope ^{59}Ni, which decays only by orbital electron capture, is absent while the daughter product of its decay, ^{59}Co, is clearly present. Figures adapted from [10].

results are shown in Figure 8. Using nucleosynthesis-yield calculations that were available at the time [12], we concluded that the lack of cosmic-ray ^{59}Ni was most likely due to decay of ^{59}Ni rather than to lack of production and ejection of this nuclide.

It has recently been pointed out [13] that more recent supernova nucleosynthesis calculations [14] that found much lower yields of ^{59}Ni have reopened the question of whether the lack of cosmic-ray ^{59}Ni clearly indicates a long time delay. Further theoretical work to reconcile the discrepant supernova nucleosynthesis results is now needed.

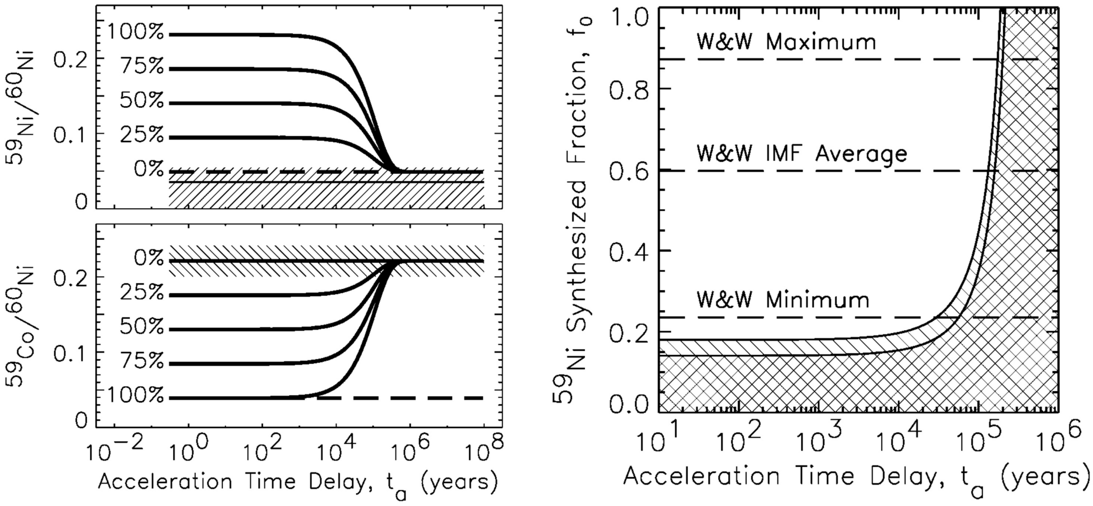

Figure 8: Left panel: calculated dependence of the ratios ^{59}Ni/^{60}Ni and ^{59}Co/^{60}Ni on the time delay between nucleosynthesis and acceleration (horizontal axis) and on the fraction of the mass-59 material synthesized as ^{59}Ni (solid lines). The dashed lines indicate the calculated contributions of secondary cosmic rays to the two ratios. The hatched regions are compatible with the CRIS isotope measurements. Right panel: Allowed regions of parameter space defined by the fraction of mass-59 material synthesized as ^{59}Ni (ordinate) and the time delay between nucleosynthesis and acceleration (abscissa). The cross-hatched region takes into account only a two standard deviation uncertainty in the measured abundances while the diagonally-hatched region also includes a 50% uncertainty in nuclear fragmentation cross sections. Figures from [10] reproduced with permission of the AAS.

3. Composition of Ultraheavy (UH) Cosmic Rays

The exposure of the CRIS instrument over the baseline ACE mission was planned to allow precise measurements of elements and isotopes up through $_{28}$Ni and exploratory measurements through $_{30}$Zn. The additional exposure made possible by the long mission duration (Fig. 4) has allowed us to extend composition studies up to $_{40}$Zr (Binns et al., in preparation). The left panel of Figure 9 shows a charge histogram for the UH region. Besides obtaining increased exposure, we have also significantly improved the rejection of backgrounds. Errors in the measured trajectories for a tiny fraction of the Fe-group events can lead to significant contamination of the UH element region because of the large abundance ratio between the Fe-group and the elements above $Z \simeq 32$. A careful study of these effects has allowed us to identify and eliminate a large fraction of such background events. For elements approaching $Z = 40$, the energies deposited in some of the CRIS detectors start to saturate the pulse-height analyzers. Uncertainties in the corrections applied to adjust for loss of events due to this saturation contribute significantly to the uncertainties in the derived abundances for these highest-Z elements.

The right panel of Figure 9 compares preliminary cosmic-ray source abundances derived from the CRIS data with published values from the SuperTIGER balloon experiment [15] and shows that there is reasonable agreement for most elements. For the highest-Z elements, further analysis of the abundance corrections and their uncertainties may lead to adjustments when the CRIS work is published.

Figure 10 shows, as a function of element mass, ratios of the GCR source abundances derived from the CRIS data to abundances in a population of matter consisting of a 94:6 mix of solar-system-like material [16] and freshly synthesized massive star material (MSM) ejected by stellar winds and supernovae [17]. In this plot, refractory and volatile elements are shown in different colors, as are log-log fits to these two element groups. This type of comparison, previously used in [18] with a somewhat different mixing ratio, organizes the data significantly better than if the GCR source composition is compared with pure solar-like composition. It has been argued [18, 15] that

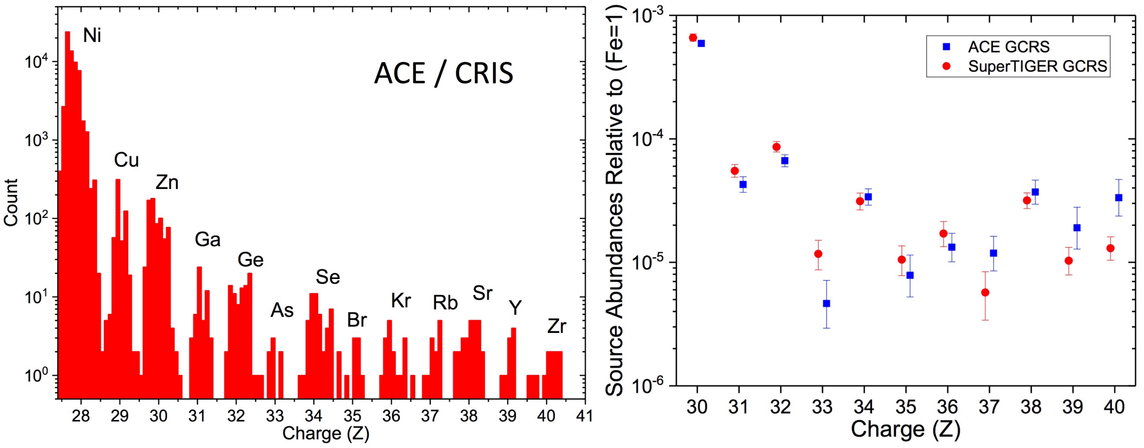

Figure 9: Left: histogram of calculated charges measured by CRIS for ultraheavy elements up through $_{40}$Zr. Right: comparison of composition in the charge range $30 \leq Z \leq 40$ measured by CRIS (blue squares) and by SuperTIGER (red circles) [15].

this organization involving a SS–MSM mix and a greater enhancement of the GCR source of refractories relative to volatiles supports the idea that cosmic rays are accelerated in OB associations where refractories are found in grains and volatiles in the gas phase.

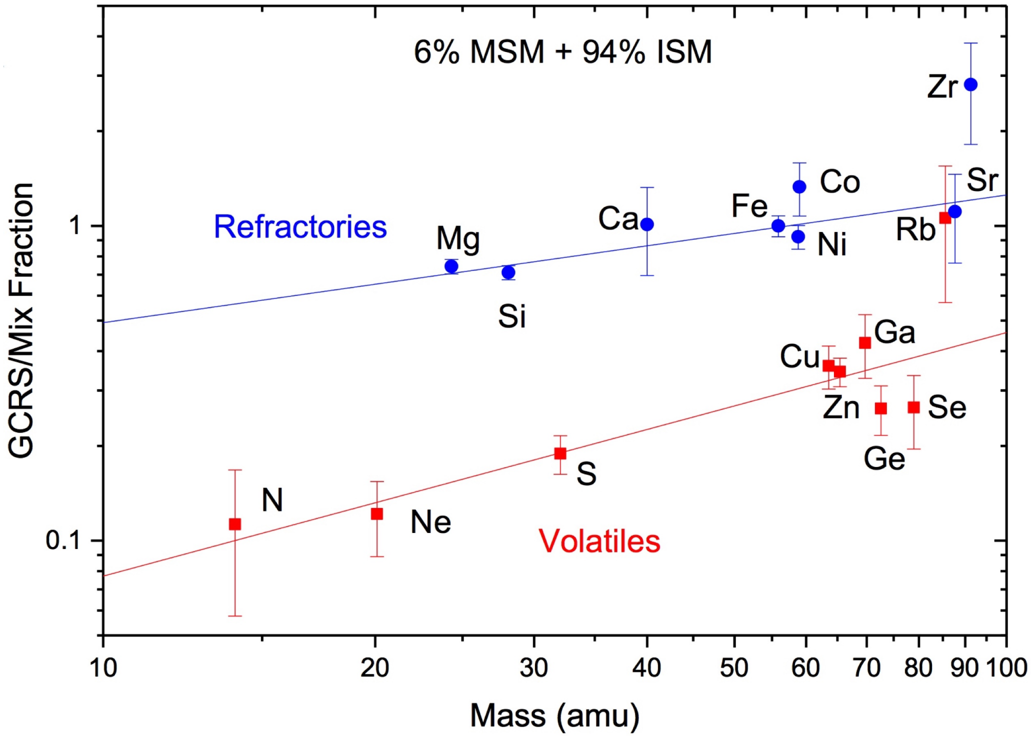

Figure 10: Ratio of GCR source abundances derived from the CRIS data to abundances calculated for an admixture of 6% massive star material (MSM) with interstellar medium material (ISM), which is assumed to have solar-like composition. Lines are log-log fits done individually to the data points for refractory and for volatile elements.

4. Solar Cycle Variation of GCR Energy Spectra

The GCR intensities measured for major heavy elements by CRIS have sufficient statistical accuracy to allow energy spectra to be derived over time scales as short as individual 27-day solar rotations. The left-hand panel of Figure 11 shows examples of Fe energy spectra measured at the lowest and highest levels of solar modulation encountered thus far during the ACE mission and also in May 2017, shortly before this writing. A fourth set of data, with an intermediate level of modulation, is shown from September 2013. The modulation at that time was found to also provide a reasonable fit to spectra at higher energies measured by the HEAO-C2 experiment in the early 1980s. The HEAO data provide an important constraint on the spectra above a few GeV/nuc where solar modulation does not cause large variations over the solar cycle. The curves that are shown were obtained from a leaky-box-model calculation of equilibrium cosmic-ray intensities in the interstellar medium followed by a solar-modulation calculation using a spherically symmetric model that includes diffusion, convection, and adiabatic deceleration. The ACE spectral measurements are at a low enough energy so that they vary significantly over the solar cycle, as well as responding to major modulation changes as can occur when large CME-driven shocks propagate out through the heliosphere. Each measured spectrum was compared with a library of template spectra from this model that differ only in the assumed modulation level, which we characterize with a “modulation parameter”, ϕ, that is calculated as described in [3].

The right-hand panel of Figure 11 shows the time dependence of the ϕ values obtained for five different elements over the entire ACE mission to date. The five curves track one another in detail, but derived ϕ values at a given time show a systematic difference that can be as large as $\sim$100 MV. These differences may be associated with the difference between the energy intervals over which the elements are measured and/or differences in the mean mass-to-charge ratios. With more sophisticated modeling, it may be possible to exploit these effects to investigate the heliospheric phenomena that control solar modulation.

A weakness in the CRIS modulation studies carried out to date is that the energy spectra in the region above a GeV/nuc are not as well constrained as at the lower energies measured with CRIS. The HEAO measurements are precise but do not come from the same time period as any of the CRIS measurements. New, precise measurements of heavy-element spectra in the GeV/nuc range that are starting to become available from PAMELA [19] and AMS-2 [20] should improve this situation.

In addition to measuring signals from heavy nuclei that stop in the CRIS detector stacks (illustrated by the trajectory shown in blue in Figure 2), the CRIS instrument also records signals from particles that penetrate an entire detector stack, as illustrated by the trajectory in red. These penetrating particles have been recorded, at a lower priority, since the beginning of the ACE mission,

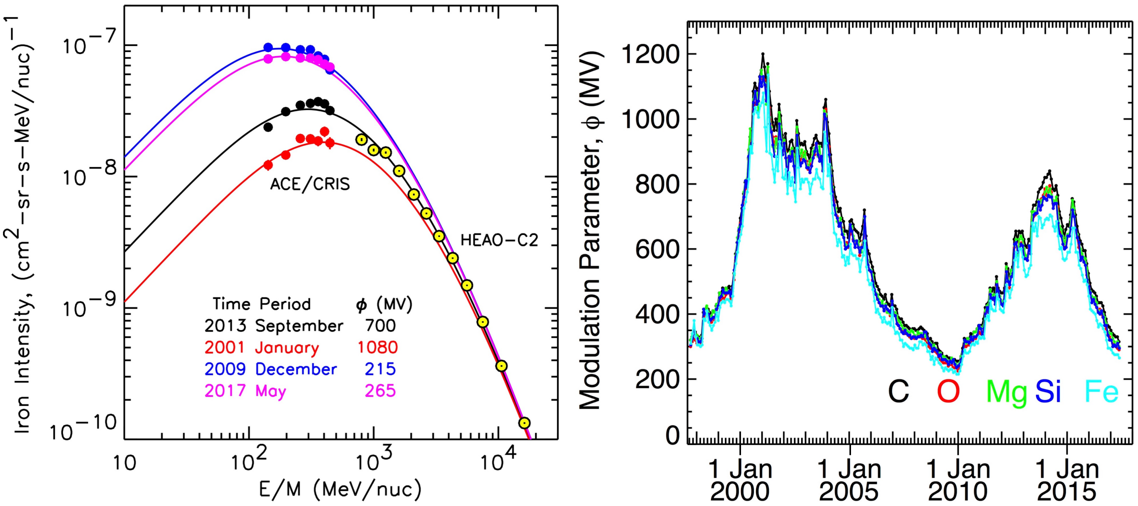

Figure 11: Left: CRIS measurements of GCR Fe energy spectra from four selected 27-day time periods, including times with the minimum and maximum levels of solar modulation observed during the ACE mission to date, one recent time period, and a time period with modulation comparable to that experienced during the HEAO mission in the early 1980s. HEAO data taken from [21]. Right: time variation of the solar modulation parameter ϕ derived by matching CRIS spectra of the type shown in the left-hand panel with calculated template spectra.

but to date they only been considered in a few exploratory studies.

In order to obtain better constraints on the energy spectra of cosmic-ray elements near the energy where the intensity maxima occur, we are developing a new analysis technique that takes advantage of these penetrating-particle data. The dE/dx versus total-E technique used for stopping particles takes advantage of the fact that the quantities E and dE/dx have different dependences on particle velocity, which separates the dE/dx-E curves for different elements, as shown in the left-hand panel of Figure 12. The dE/dx-E technique is not directly applicable for penetrating particles because the total energy is not measured. However, since dE/dx and the second derivative, d^2E/dx^2, also have different velocity dependences, one can develop a similar analysis method based on these two parameters, as shown in the right-hand panel of Figure 12.

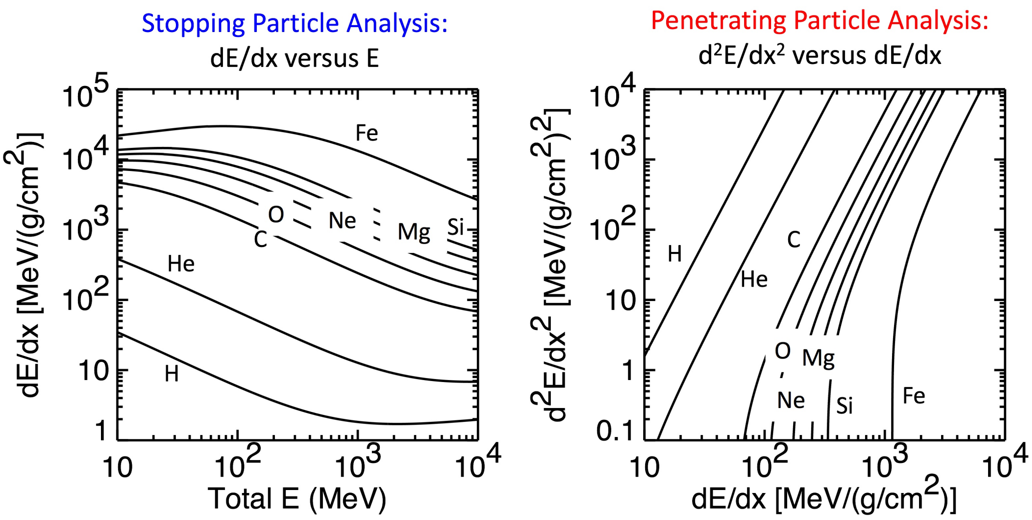

Figure 12: Plots of dE/dx versus E (left) and d^2E/dx^2 versus dE/dx (right) derived from a standard heavy-ion range-energy relation illustrate the approaches used for resolving elements in the stopping- and penetrating-particle data sets.

To obtain a measure of d^2E/dx^2, we compare the energy losses in detector E1, at the front of the stack, and E8, near the back of the stack (see Figure 2). This is used in conjunction with the sum of the energies deposited in all of the stack detectors from E1 through E8, which we divide by $\sec\theta$ to account for the angular variation of the thickness of silicon penetrated. The left-hand panel of Figure 13 illustrates the application of this analysis technique to CRIS angle-selected penetrating-particle data collected during 2009. The element tracks at a given angle of incidence are well resolved over much of the plot, but there is a spread among the tracks for a given element at different angles. A simple correction for incidence angle can be applied to approximately map all of the tracks onto the track for $\theta = 0^\circ$, as illustrated in the right-hand panel. In the high-energy region at the bottom of the plot (ordinate values $\lesssim$0.2) there is overlap between tracks, as is most easily seen near the bottom of the track for $_{24}$Cr, where there is an enhanced density of points. Geant4 simulations have shown that this is due to relativistic $_{26}$Fe that produces high-energy knock-on electrons that penetrate into detectors deeper in the stack and increase the energy deposited in E8. This region is also affected by the relativistic rise in dE/dx. It may be possible to improve the

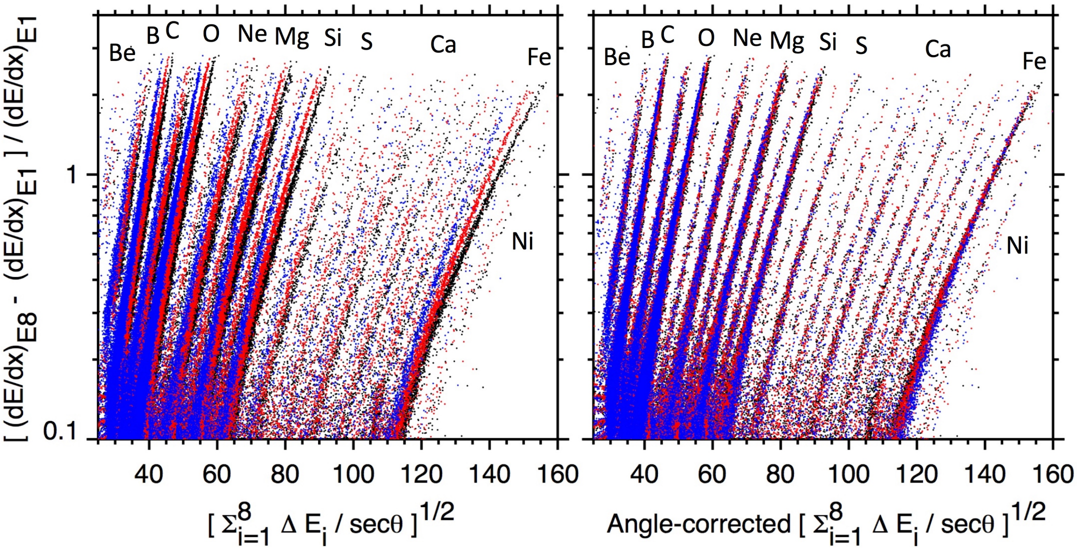

Figure 13: Scatter plots constructed using parameters that produce resolved element tracks for penetrating nuclei. Energies are in MeV. The data plotted were collected by CRIS during the solar minimum year 2009. Events are included from three narrow ranges of incidence angle, as indicated by color: black, 0°–7°; red, 29°–31°; blue, 43°–47°. Left: no θ correction applied other than the explicit division by $\sec\theta$ in abscissa. Right: same data with θ-dependent corrections applied to approximately map all of the data onto the $\theta = 0°$ tracks.

resolution in this region by comparing the energies measured in the other detectors to the pattern expected from deposited-energy calculations.

Once a particle's atomic number has been identified from the location at which the event falls on a plot like Figure 13, its incident energy per nucleon can be calculated from the range–energy relation using as inputs the total thickness penetrated in the detector stack and the energy deposited in that thickness. This calculation depends on the particle's mass. As a first approximation, the mass can be assumed to be that of the most abundant isotope of the element, but that will introduce a mass-dependent error in the derived E/M values for events falling in the upper part of Figure 13. Ultimately, it will be necessary to correct derived energy spectra using isotopic composition information, which is available from the stopping-particle data.

Figure 14 shows examples of combined CRIS stopping- and penetrating-particle energy spectra for O and Fe at solar minimum (2009). The calculation of absolute intensities from the numbers of penetrating particle events detected requires a correction for inefficiencies in the transmission of these events to the ground. The bit-rate assigned to CRIS is sufficient to transmit all of the stopping, high-Z events, which are assigned the highest priority, but only a fraction of the lower-priority penetrating events. Counts of numbers of events detected and telemetered are maintained for each priority and can be used to correct for the events that could not be transmitted. Since we are still working on developing and validating these corrections, the penetrating-particle portions of the spectra in Figure 14 have been normalized to match the extrapolation from the highest energy points in the stopping portion.

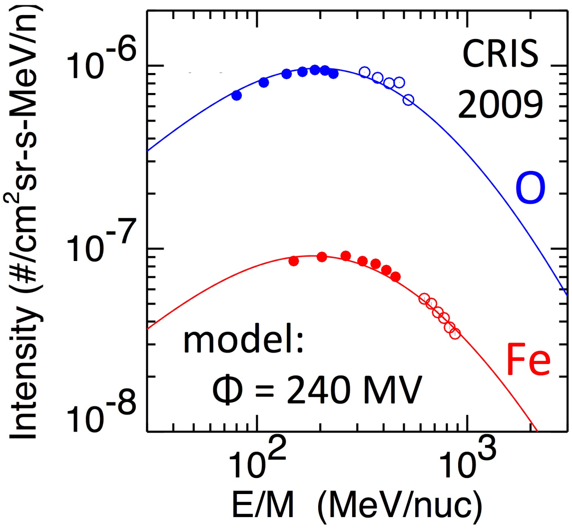

Figure 14: Points: preliminary energy spectra of Fe and O measured by CRIS for the solar minimum year 2009. The stopping points (filled circles) are from level 2 data available from the ACE Science Center. The penetrating points (open circles) are derived using the new analysis technique. The absolute normalization of the penetrating spectra was adjusted to approximately match the extrapolation of the stopping spectra using a common scale factor for both O and Fe. The derivation of the absolute normalization for the penetrating particle intensities is presently being worked on by the CRIS team.

5. Summary and Conclusions

For the past 20 years, data from the CRIS instrument on ACE have been providing precise, near-Earth measurements of galactic cosmic-ray elemental and isotopic composition, and also of energy spectra near the intensity maximum. Recent advances include: 1) detecting, for the first time, a surviving primary radionuclide, ^{60}Fe; 2) providing further evidence that cosmic-ray source composition is well represented by a mass-dependent fractionation of a parent population of matter consisting of a mix of massive star material with old, solar-like ISM from which refractory elements are extracted with efficiencies that are enhanced by about a factor of four relative to those for volatile elements; and 3) determining the time variation of solar modulation over nearly two full solar cycles using energy spectra of multiple heavy elements.

The ACE spacecraft is capable of operating well into the maximum of solar cycle 25 and is expected to provide measurements that will be important for interpreting data from NASA's Parker Solar Probe and ESA's Solar Orbiter missions, which are scheduled to be launched in 2018, as well as continuing to monitor space weather in the near-Earth environment.

Acknowledgments

We thank G. Morlino and V. Ptuskin for helpful comments on the application of propagation models to derive of the source ratio ^{60}Fe/^{56}Fe.

The research was carried out with support from the National Aeronautics and Space Administration at the California Institute of Technology (under grant NNX13AH66G), the Jet Propulsion Laboratory, Washington University in St. Louis, and the Goddard Space Flight Center.

References

[1] C. T. Russell, R. A. Mewaldt, & T. T. von Rosenvinge (eds.), *The Advanced Composition Explorer Mission*, (Kluwer: Dordrecht), reprinted from *Space Science Reviews* 86, Nos. 1–4, 1998.

[2] E. C. Stone et al., *The Cosmic-Ray Isotope Spectrometer for the Advanced Composition Explorer*, *Space Sci. Rev.*, **86**, 285, 1998.

[3] K. A. Lave et al., *Galactic Cosmic-Ray Energy Spectra and Composition During the 2009–2010 Solar Minimum Period*, *ApJ*, **770**, 117, 2013.

[4] M. E. Wiedenbeck et al., *The Origin of Primary Cosmic Rays: Constraints from ACE Elemental and Isotopic Composition Observations*, *Space Sci. Rev.*, **99**, 15, 2001.

[5] E. C. Stone et al., *The Solar Isotope Spectrometer for the Advanced Composition Explorer*, *Space Sci. Rev.*, **86**, 357, 1998.

[6] W. R. Binns et al., *Observation of the ^{60}Fe Nucleosynthesis-Clock Isotope in Galactic Cosmic Rays*, *Science*, **352**, 677, 2016.

[7] N. E. Yanasak et al., *Measurement of the Secondary Radionuclides ^{10}Be, ^{26}Al, ^{36}Cl, ^{54}Mn, and ^{14}C and Implications for the Galactic Cosmic-Ray Age*, *ApJ*, **563**, 768, 2001.

[8] A. W. Strong, I. V. Moskalenko, & V. S. Ptuskin, *Cosmic-Ray Propagation and Interactions in the Galaxy*, *Ann. Rev. Nucl. Part. Sci.*, **57**, 285, 2007.

[9] B. J. Fry, B. D. Fields, & J. R. Ellis, *Radioactive Iron Rain: Transporting ^{60}Fe in Supernova Dust to the Ocean Floor*, *ApJ*, **827**, 48, 2016.

[10] M. E. Wiedenbeck et al., *Constraints on the Time Delay between Nucleosynthesis and Cosmic-ray Acceleration from Observations of ^{59}Ni and ^{59}Co*, *ApJL*, **523**, L61, 1999.

[11] A. Soutoul, M. Cassé, & E. Juliusson, *Time Delay between the Nucleosynthesis of Cosmic Rays and their Acceleration to Relativistic Energies*, *ApJ*, **219**, 753, 1978.

[12] S. E. Woosley & T. A. Weaver, *The Evolution and Explosion of Massive Stars. II. Explosive Hydrodynamics and Nucleosynthesis*, *ApJS*, **101**, 181, 1995.

[13] A. Neronov & G. Meynet, *Abundances of ^{59}Co and ^{59}Ni in the Cosmic-ray Flux*, *A&A*, **588**, A86, 2016.

[14] A. Chieffi & M. Limongi, *Pre-supernova Evolution of Rotating Solar Metallicity Stars in the Mass Range 13–120$M_\odot$ and their Explosive Yields*, *ApJ*, **764**, 21, 2013.

[15] R. P. Murphy et al., *Galactic Cosmic Ray Origins and OB Associations: Evidence from SuperTIGER Observations of Elements $_{26}$Fe through $_{40}$Zr*, *ApJ*, **831**, 148, 2016.

[16] K. Lodders, *Solar System Abundances and Condensation Temperatures of the Elements*, *ApJ*, **591**, 1220, 2003.

[17] S. E. Woosley & A. Heger, *Nucleosynthesis and Remnants in Massive Stars of Solar Metallicity*, *Phys. Reports*, **442**, 269, 2007.

[18] B. F. Rauch et al., *Cosmic Ray Origin in OB Associations and Preferential Acceleration of Refractory Elements: Evidence from Abundances of Elements $_{26}$Fe through $_{34}$Se*, *ApJ*, **697**, 2083, 2009.

[19] O. Adriani et al., *Measurement of Boron and Carbon Fluxes in Cosmic Rays with the PAMELA Experiment*, *ApJ*, **791**, 93, 2014.

[20] E. Fiandrini, *Precision Measurements of Nuclear CR Energy Spectra and Composition with the AMS-02 Experiment*, *J. Phys. Conf. Ser.*, **718**, 052012, 2016.

[21] J. J. Engelmann et al., *Charge Composition and Energy Spectra of Cosmic-ray Nuclei for Elements from Be to Ni. Results from HEAO-3-C2*, *A&A*, **233**, 96, 1990.